DOI: 10.1002/chem.201000461

Near-IR Core-Substituted Naphthalenediimide Fluorescent Chemosensors for Zinc Ions: Ligand Effects on PET and ICT Channels

Xinyu Lu,[a] Weihong Zhu,*[a] Yongshu Xie,[a] Xin Li,[a] Yuan Gao,[b] Fuyou Li,[b] and He Tian*[a]

Abstract: Near-IR (NIR) emission can offer distinct advantages for both in vitro and in vivo biological applications. Two NIR fluorescent turn-on sensors *N*,*N*′-di-*n*-butyl-2-(*N*-{2-[bis-(pyridin-2-ylmethyl)amino]ethyl})-6-(*N*-piperidinyl)naphthalene-1,4,5,8-tetracarboxylic acid bisimide and *N*,*N*′-di-*n*-butyl-2-[*N*,*N*,*N*′-tri(pyridin-2-ylmethyl)amino]ethyl-6-(*N*-piperidinyl)naphthalene-1,4,5,8-tetracarboxylic acid bisimide (PND and PNT) for Zn^{2+} based on naphthalenediimide fluorophore are reported. Our strategy was to choose core-substituted naphthalenediimide (NDI) as a novel NIR fluorophore and *N*,*N*-di(pyridin-2-ylmethyl)ethane-1,2-diamine (DPEA) or *N*,*N*,*N*′-tri(pyridin-2-ylmethyl)ethane-1,2-diamine (TPEA) as the receptor, respectively, so as to improve the selectivity to Zn^{2+}. In the case of PND, the negligible shift in absorption and emission spectra is strongly suggestive that the secondary nitrogen atom (directly connected to the NDI moiety, N^1) is little disturbed with Zn^{2+}. The fluorescence enhancement of PND with Zn^{2+} titration is dominated with a typical photoinduced electron-transfer (PET) process. In contrast, the N^1 atom for PNT can participate in the coordination of Zn^{2+} ion, diminishing the electron delocalization of the NDI moiety and resulting in intramolecular charge-transfer (ICT) disturbance. For PNT, the distinct blue-shift in both absorbance and fluorescence is indicative of a combination of PET and ICT processes, which unexpectedly decreases the sensitivity to Zn^{2+}. Due to the differential binding mode caused by the ligand effect, PND shows excellent selectivity to Zn^{2+} over other metal ions, with a larger fluorescent enhancement centered at 650 nm. Also both PND and PNT were successfully used to image intracellular Zn^{2+} ions in the living KB cells.

Keywords: fluorescent sensors · ligand effects · naphthalene diimides · NMR spectroscopy · zinc

Introduction

As the second most abundant transition metal in the human body, the zinc ion plays a great role in biological systems, such as DNA binding, apoptosis, signal transduction, gene expression, metalloenzyme catalysis, and neurotransmission.[1] It is well-believed that the lack of zinc ions could result in an increasing risk of several diseases.[2] Therefore, it is necessary to get an insight into the vital roles of Zn^{2+} in biological processes with the growing demand for sensing Zn^{2+} in living systems. For this purpose, a variety of fluorescent Zn^{2+} sensors have been documented based on various fluorophores, such as acridine, anthracene, benzoxazole, boradiazaindacene, coumarin, dansyl, fluorescein, naphthalimide, nitrobenzoxadiazole, quinoline, or squaraines.[3] For example, Lippard et al. have reported several series of zinc probes by making alterations to a Zn^{2+}-binding unit and fluorophore platform, and even successfully imaged the distribution, uptake, and mobilization of Zn^{2+} in various types of cells and neuronal cultures.[4] However, the cases on Zn^{2+} sensors in the near-IR (NIR) fluorescent emission between 650 and 900 nm are still less common.[5] As a matter of fact, such longer wavelength emission can offer distinct advantages for both in vitro and in vivo biological applications in that they can avoid the strong interference from UV-induced phototoxicity/autofluorescence and sensor-induced in-

[a] X. Lu, Prof. Dr. W. Zhu, Prof. Dr. Y. Xie, X. Li, Prof. Dr. H. Tian
Key Laboratory for Advanced Materials and
Institute of Fine Chemicals
East China University of Science and Technology
Shanghai 200237 (P. R. China)
Fax: (+86) 21-6425-2758
E-mail: whzhu@ecust.edu.cn
tianhe@ecust.edu.cn

[b] Y. Gao, Prof. Dr. F. Li
Department of Chemistry & Laboratory of
Advanced Materials, Fudan University
Handan Road 220, Shanghai 200433 (P. R. China)

Supporting information for this article is available on the WWW under http://dx.doi.org/10.1002/chem.201000461.

terference encountered in the shorter wavelength region. In this regard, it is highly desirable to develop Zn^{2+}-selective NIR fluorescent sensors to match harmless imaging and visualization of Zn^{2+} in living cells.

With these considerations in mind, we designed and synthesized two novel NIR fluorescent turn-on sensors *N*,*N*′-di-*n*-butyl-2-(*N*-{2-[bis(pyridin-2-ylmethyl)amino]ethyl})-6-(*N*-piperidinyl)naphthalene-1,4,5,8-tetracarboxylic acid bisimide and *N*,*N*′-di-*n*-butyl-2-[*N*,*N*,*N*′-tri(pyridin-2-ylmethyl)amino]ethyl-6-(*N*-piperidinyl)naphtalene-1,4,5,8-tetracarboxylic acid bisimide (PND and PNT) for Zn^{2+} ion based on naphthalenediimide fluorophore (NDI). Also a piperidine unit was incorporated as a strong electron-donor to the NDI core by nucleophilic substitution for extending the push–pull electronic system with an emission band centered at 650 nm, thus successfully tuning the determining wavelength to fall in the desirable NIR region. Furthermore, among the available ionophore groups, two water-compatible and membrane-permeable chelators, *N*,*N*-di(pyridin-2-ylmethyl)-ethane-1,2-diamine (DPEA)[6] and *N*,*N*,*N*′-tri(pyridin-2-ylmethyl)ethane-1,2-diamine (TPEA),[7] were incorporated for considering the selectivity of Zn^{2+} over other metal ions under physiological conditions.[3i,8a,9] With respect to the dipyridine amine unit in the ligand of DPEA, the additional pyridine in the ligand of TPEA might be expected to improve the selectivity due to the effect of cooperative chelating. Interestingly, in the target sensors of PND and PNT, two ionophores exhibit completely different ligand effects on photoinduced electron-transfer (PET) and intramolecular charge-transfer (ICT) channels due to the different coordination behavior between DPEA and TPEA. Unexpectedly, upon comparing with PNT, competition experiments demonstrate that PND shows higher selectivity to Zn^{2+} with less interference by Cd^{2+}.

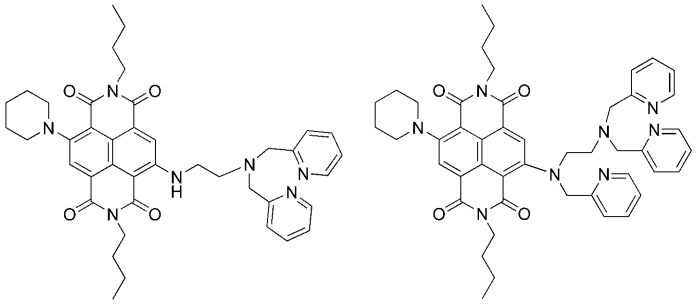

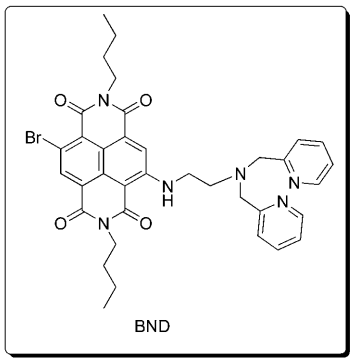

Results and Discussion

Design and synthesis of PND and PNT: NDI is an exquisite building block for supramolecular self-assemblies,[10] excellent n-type semiconductors for organic field-effect transistors (OFETs),[11] and n-type functional materials (electron acceptor) for solar energy conversion materials.[12] Considering their richness in spectroscopic and electrochemical properties, NDI derivatives are ideally suitable for sensor design. Recently, two NDI-based fluorescent-ion sensors through forming excimers have been reported.[13] Generally, most functionalizations of NDI are through its dianhydride group or core substitution at the 2-, 3-, 6- and/or, 7-position, providing a facial way to tune the emission wavelength from 387 to 623 nm,[14a] even longer than 650 nm[14b,c] (falling into the NIR region). Meanwhile, the hydrophilic, lipophilic, or biophilic unit can be easily incorporated into the specific NDI chromophore for developing novel NIR fluorescent systems to meet a variety of requirements in chemical and biological analysis.

In our synthesis, we first attempted to incorporate the ligand unit at both the 2- and 6-positions of the NDI core for preparing a symmetric chelate-appended sensor. Due to the easy cleavage of the pyridylmethyl carbon–nitrogen bond in DPEA or TPEA, we prefer to treat *N*,*N*′-dibutyl-2,6-dibromonaphthalene bisimide (**2**) with the ligand at moderate temperature (Scheme 1). Unfortunately, only one bromo group can be substituted with the ligands of DPEA or TPEA at 60 °C. It was very difficult to introduce a second

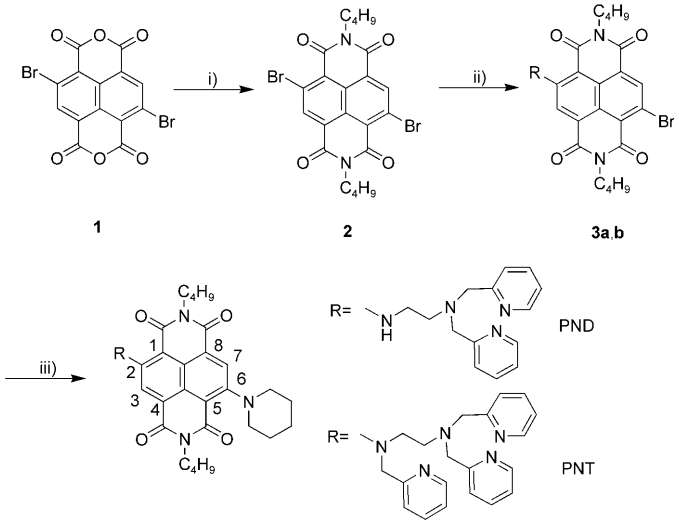

Scheme 1. Synthetic route of target sensors: i) *n*-butylamine, acetic acid, 118 °C, 5 h, 58 %; ii) DPEA or TPEA, NMP, 60 °C, 70 h; iii) piperidine, NMP, 50 °C, 24 h.

ligand to the NDI core, which might be due to the poor reactivity of the aliphatic amines in the DPEA or TPEA ligand. When using a more reactive and nucleophilic piperidine group, the remaining bromo group in the core of NDI can be successfully substituted (Scheme 1). As expected, the second substituted piperidine group with strong electron-donating capability plays an essential role in realizing a large bathochromic shift, thus obtaining target sensors with the emission located at the NIR region.

As illustrated in Scheme 1, the target molecules of PND were conveniently synthesized by three steps from 2,6-dibromonaphthalene bisanhydride (**1**), which was prepared according to the published procedure.[15] Firstly, compound **1** was treated with *n*-butylamine in hot acetic acid under reflux to give *N*,*N*′-dibutyl-2,6-dibromonaphthalene bisimide (**2**) in 58% yield. In the following steps, by using triethylamine as an acid-trap agent in dry *N*-methyl-2-pyrrollidone (NMP), the two bromo groups of intermediate **2** were nucleophilically stepwise-substituted with DPEA and piperidine, respectively, to give the target core-substituted Zn^{2+} sensor PND with a yield of 31%. Similarly, **2** was treated with TPEA instead of DPEA at the second step, which finally resulted in PNT with a yield of 33%. The chemical structures of PND and PNT were fully characterized by ^{1}H and ^{13}C NMR spectroscopy and HRMS as shown in the Experimental Section.

Optical properties of BND, PND, and PNT: By using the monosubstituted intermediate as a reference (*N*,*N*′-di-*n*-butyl-2-(*N*-{2-[bis(pyridin-2-ylmethyl)amino]ethyl})-6-bromonaphthalene-1,4,5,8-tetracarboxylic acid bisimide (BND)), the normalized absorption and fluorescence spectra of sensors PND and PNT in chloroform were initially studied (Figure 1). All of them display a characteristic intense absorption band corresponding to the core-substituted naphthalenediimide moiety in the visible region.[16] With respect to BND in the UV region, both PND and PNT exhibit two similar intense absorption bands located at about 356 and 374 nm, which have little effect on the core substituents. Meanwhile, upon comparison with the absorption band of BND (located at 528 nm) in the visible region, PND and PNT exhibit obviously bathochromic shifts of 72 and 77 nm, respectively, which are accompanied by a distinct color change from red to dark blue (see Figure S1 in the Supporting Information). A similar change in the emission can be also observed, that is, there is a bathochromic shift from the monosubstituted BND (λ_{em} 565 nm) to the disubstituted PND (λ_{em} 644 nm) and PNT (λ_{em} 638 nm). Clearly, the incorporation of a piperidine group at the 6-position of the NDI-core by nucleophilic displacement can extend the push–pull electronic system with positive mesomeric effects (+*M* effect, bathochromic shift)[14b] on both absorption and emission, thus successfully tuning the wavelength to fall in the desirable long-wavelength region.

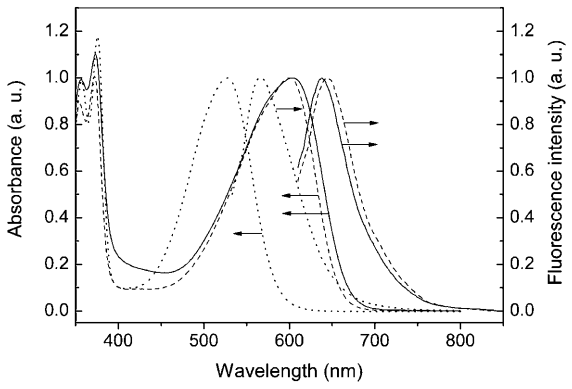

Figure 1. Normalized absorption and fluorescence spectra of BND (•••••), PND (-----), and PNT (——) in chloroform (2.0×10^{-5} M).

Absorption and fluorescence response of PND and PNT to Zn^{2+}: Spectroscopic response measurements with PND and PNT were studied in a mixture of acetone/water (90:10, v/v) with a buffer solution of 3-(*N*-morpholino)propanesulfonic acid (MOPS, 10 mM, pH 7.0). Notably in buffered acetone/water solution, PND shows a bathochromic shift of 6 nm in emission to 650 nm due to the solvent effect, and a similar change in the absorption and emission of PNT can be also observed (see Table S1 in the Supporting Information).

Titrations of PND and PNT with Zn^{2+} were then performed in MOPS buffer system to characterize Zn^{2+} coordination. As shown in Figure 2A, the absorption band of free PND exhibits a maximum centered at 610 nm. Upon adding one equivalent of Zn^{2+}, the absorption band and intensity

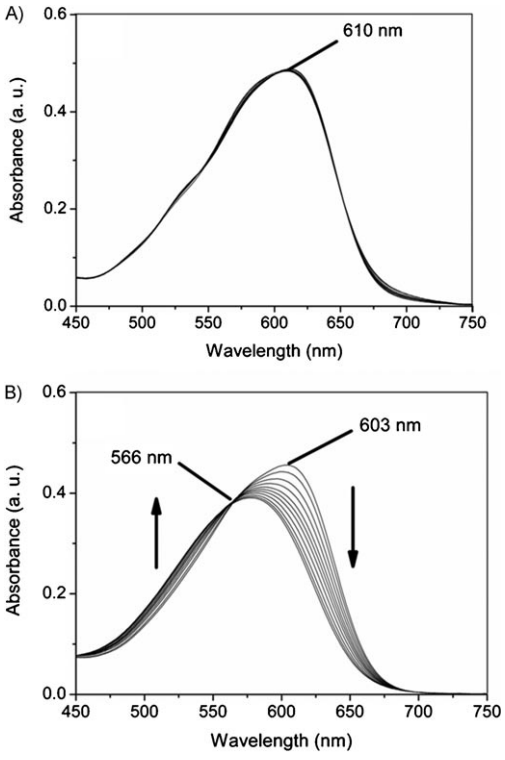

Figure 2. Changes in absorption spectra upon titration of Zn^{2+} from 0 to 1.0 equiv: A) PND (50 μM). B) PNT (50 μM). All data were obtained in aqueous solution (acetone/100 mM MOPS buffer 90:10, pH 7.0).

did not change. To understand the interaction between PND and Zn^{2+}, the fluorescence titration with Zn^{2+} was also monitored. When excited at 610 nm, there is a very small blueshift of 3 nm in the emission peak wavelength for PND with a sequential addition of Zn^{2+}, but showing a turn-on fluorescent response with zinc addition (Figure 3A). When

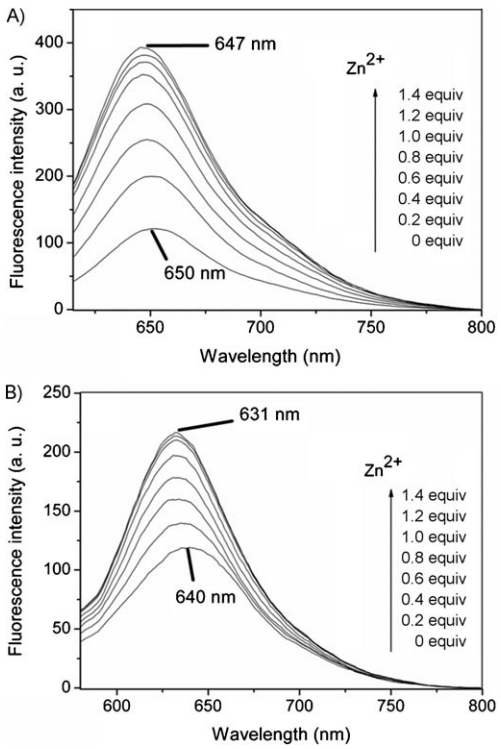

Figure 3. Changes in fluorescence spectra upon titration of Zn^{2+} from 0 to 1.4 equiv: A) PND (50 μM, $\lambda_{ex}=610$ nm). B) PNT (50 μM, $\lambda_{ex}=566$ nm). All data were obtained in aqueous solution (acetone/100 mM MOPS buffer = 90:10, pH 7.0).

adding more than one equivalent of Zn^{2+}, the maximum of fluorescence intensity at 647 nm is reached (Table 1). It also shows a fast fluorescent response within less than 20 s (see Figure S2 in the Supporting Information). The fluorescence enhancement of PND during the titration with Zn^{2+} is a typical PET characteristic. It is blocking PET[8] from the lone electron pair of the tertiary nitrogen atom (dipicolylamine, N^2) in the NDI fluorophore (Scheme 2A). Furthermore in the case of PND, the neglect of a shift in absorption and emission spectra strongly suggested that the secondary nitrogen atom (directly connected to the NDI moiety, N^1) is little disturbed by Zn^{2+}, that is, the coordination between Zn^{2+} and N^1 can be possibly ruled out.

Table 1. Optical properties of PND, PNT, and their zinc complexes.[a]

Systems	Absorption peak λ_{ab} [nm]	Extinction coefficient [$\times 10^3\,M^{-1}cm^{-1}$]	Emission peak λ_{em} [nm]	Fluorescence yield Φ_{em}[b]
PND	610	9.74	650	0.17
PND + Zn^{2+}[c]	610	9.72	647	0.55
PNT	603	9.12	640	0.23
PNT + Zn^{2+}[c]	577	7.81	631	0.42

[a] All data were obtained in aqueous solution (acetone/100 mM MOPS buffer 90:10, pH 7.0). [b] Fluorescent quantum yields were determined in reference to *N*,*N*′-di(2,6-dibutyl)-1,6,7,12-tetrakis(4-*tert*-butylphenoxy)-3,4:9,10-perylenetetracarboxylic diimide ($\Phi=0.66$, in CH_2Cl_2).[17] [c] The data were measured in the presence of Zn^{2+} (1.0 equiv with respect to PND or PNT).

On the other hand, PNT undergoes different phenomena, that is, a large blueshift in both absorption and emission peak is observed. Upon adding one equivalent of Zn^{2+} into the PNT system, the absorption peak at 603 nm became decreased, and simultaneously a blueshifted absorption peak centered at 577 nm was developed with a well-defined isosbestic point at 566 nm (Figure 2B, Table 1). Upon choosing the isosbestic point as the excitation wavelength, the emission intensity of PNT was also enhanced to some extent with a distinct blueshift from 640 to 631 nm upon the sequential addition of Zn^{2+} (Figure 3B). Such a blueshift means that the nitrogen N^1 attached to the NDI moiety is disturbed with Zn^{2+}, thus resulting in a decrease in the electron-donating ability. Here, upon comparing with PND, the nitrogen atom N^1 for PNT shows a much stronger coordination tendency with Zn^{2+}. This might be attributed to the additional pyridinyl nitrogen N^5 in TPEA, which helps N^1–N^4 to form a five-coordinating Zn^{2+} complex by a synergistic chelating effect (Scheme 2B). Consequently, the moderate "off–on" enhancement and the distinct blueshift in both absorption and emission peak for PNT is suggestive of a combination of PET and ICT processes[7d], which unexpectedly decreases the sensitivity to Zn^{2+}.

pH effects on the fluorescence of PND and PNT were also examined (Figure 4). For PND, the weak emission (λ_{em} at 650 nm) was observed with the excitation at 610 nm. Its emission intensity does not change significantly in the range of pH 6.0–9.0. However, a distinct emission enhancement of three-fold at 650 nm can be observed when decreasing the pH from 6.0 to 3.0 (Figure 4), which shows a typical PET block caused by the protonation of the nitrogen atom N^2[18] and a negligible induced PET process caused by the protonation of pyridine subunits[8b,c] (see Figure S3A in the Supporting Information). On the other hand, the fluorescence intensity of PNT ($\lambda_{em}=635$ nm) does not change as significantly as PND in the range of pH 3.0–9.0 ($\lambda_{ex}=566$ nm, see Figure S3B in the Supporting Information). Again, the decreased sensitivity to low pH for PNT suggests a dominated control of ICT[9] with some degree of PET process. Notably, the stable fluorescence of PND and PNT at around pH 7.0 is favorable for in vivo application.

^{1}H NMR titration of PND and PNT with Zn^{2+}: Interestingly, the target sensors of PND and PNT exhibit different optical properties due to different coordination modes of Zn^{2+}, respectively. Actually, their binding behaviors are more pronounced with NMR titration in [D_6]DMSO. As shown in Figure 5, upon adding an increasing amount of Zn^{2+}, another set of NMR spectroscopic signals for the Zn^{2+}-coordination complex appears besides the set of signals for free

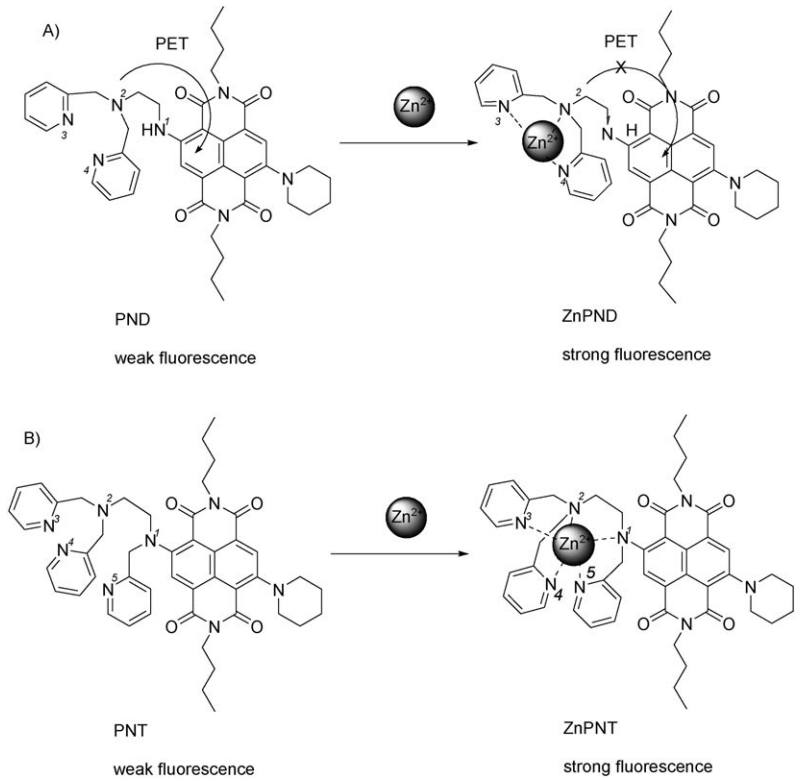

Scheme 2. Proposed Zn^{2+} binding mode: A) PND and B) PNT (note: in the case of PND, the neglect of a shift in absorption and emission spectra strongly suggested that the secondary nitrogen atom (directly connected to the NDI moiety, N^1) is little disturbed by Zn^{2+}, that is, the coordination between Zn^{2+} and N^1 can be possibly ruled out).

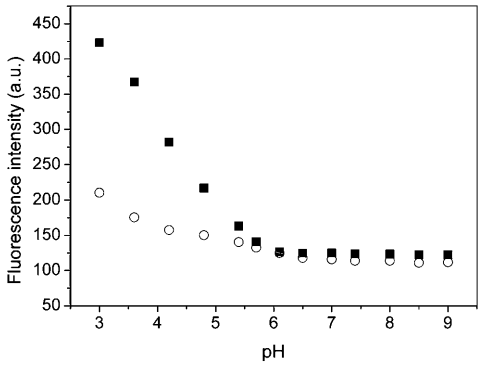

Figure 4. Effect of pH on the fluorescence intensity of PND (■, 50 μM) and PNT (○, 50 μM) in 0.1 M sodium phosphate solution adjusted to various pH values, which was determined at 650 nm with an excitation at 610 nm for PND, and at 635 nm with excitation at 577 nm for PNT.

probes. When 0.5 equivalents of Zn^{2+} was added, two sets of NMR spectroscopic signals display almost identical intensity, whereas when one equivalents of Zn^{2+} was added, only the signals corresponding to the complex can be observed. However, more equivalents of Zn^{2+} does not lead to any further evident change in the ^1H NMR spectrum, which is indicative of the 1:1 binding ratio.

The chemical shifts in Zn^{2+} complexes are also compared with those in free probes of PND and PNT (Figure 5, see Tables S2 and S3 in the Supporting Information). For probe PND, Zn^{2+} coordination triggers a clear downfield shift of H_a in the pyridine unit from $\delta =$ 8.45 to 8.62 ppm. The signal for H_b of pyridine groups show a significant downfield shift up to $\Delta\delta = 0.88$ ppm, whereas the signals for H_c and H_d in pyridine at about $\delta 7.6$ ppm were almost unchanged, which is consistent with the previous observation,[3i] indicative of the possible direction of charge transfer from the pyridine to Zn^{2+}. As for the methylene hydrogen (H_e), the singlet at $\delta = 3.86$ ppm splits into two doublets at $\delta = 4.13$ and 4.50 ppm, respectively. It might be attributed to two different proton environments, one of them much more affected by the presence of Zn^{2+} probably by closer proximity.[19] Meanwhile, a triplet for H_f at $\delta = 2.88$ ppm also shows an obvious downfield shift by $\delta =$ 0.15 ppm, which indicates that the tertiary amino-N^2 adjacent to the methylene are strongly bonded with Zn^{2+}. The singlet for H_h at $\delta = 9.75$ ppm corresponding to the N^1H of PND disappeared upon titration of Zn^{2+}, mainly due to the active proton exchanged with trace water. In addition, the slightly downfield shift for H_i and H_j of the NDI moiety by $\delta = 0.11$ and 0.07 ppm, respectively, is indicative of little change in charge density on the core of PND during its binding with Zn^{2+}.

Compared with PND, H_{a-d} in pyridines of PNT show a similar downfield shift upon the titration of one equivalent of Zn^{2+}. Notably, the triplets for H_g of PNT shift downfield with a $\Delta\delta$ of 0.51 ppm, much larger than that of PND ($\Delta\delta$ of 0.26 ppm for H_g in the case of PND), also supporting a stronger coordination occurring between Zn^{2+} and tertiary amino N^1 of PNT than that of PND. This difference is exactly consistent with the phenomena in absorption and emission spectra.

Again, the DFT calculation by the Gaussian 03 software package demonstrated two different coordination modes for Zn^{2+}–PND and Zn^{2+}–PNT in support of the proposed binding process. As shown in Figure S4 and Table S4 in the Supporting Information, the bonding lengths of N–Zn are close to the reported ones[20] in the optimized structures. In the case of the Zn^{2+}–PND complex, the Zn^{2+} ion is chelated by the DPEA unit with the participation of possible anions (for example, nitrate anions), thus leaving the N^1 atom alone, not directly coordinated with Zn^{2+}. This is why PET domi-

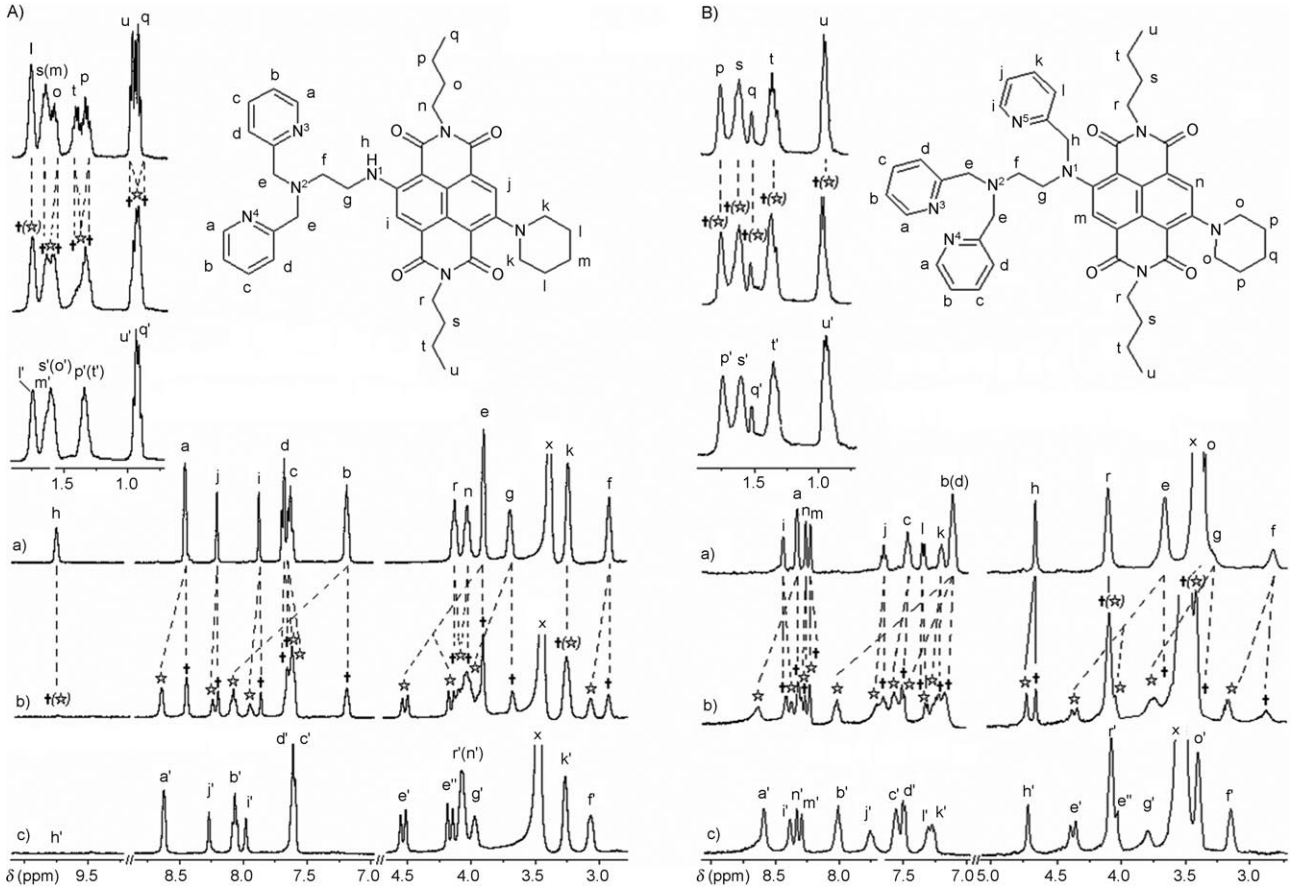

Figure 5. Partial ^{1}H NMR spectra (400 MHz, [D$_6$]DMSO) in the absence (a) and in the presence of b) 0.5 and c) 1.0 equiv of Zn^{2+}: A) PND (5 mM) and B) PNT (5 mM). The signals marked with +, ☆, and × are for the protons from the free sensor, zinc-bound sensor, and H_2O, respectively.

nates with the negligible shift in absorption and emission spectra of PND. In contrast, in the Zn^{2+}–PNT complex, the N^1 atom can participate in the coordination of the Zn^{2+} ion. And the N^1 amine group is found to be perpendicular to the naphthalene plane, which diminishes the electron delocalization of the NDI moiety for PNT, and results in the ICT disturbance to tune the blueshift in both absorbance and fluorescence.

Zn^{2+} selectivity, competition experiments, and in vivo imaging: Job plot analyses of Zn^{2+} with PND or PNT were also performed with fluorescence. Both of them show breaks at 0.5, indicative of a same 1:1 binding behavior in solution (see Figure S5 in the Supporting Information). Moreover, the apparent association constants (K_{ass}) of Zn^{2+} with PND and PNT were determined to be $2.3(\pm0.3)\times10^5$ and $1.6(\pm0.4)\times10^6\,M^{-1}$, respectively, by a nonlinear least-square fitting of the fluorescence data (see Figure S6 in the Supporting Information). As expected, the K_{ass} for PNT is larger by almost one order of magnitude than that for PND since the cooperative coordination induced by the additional pyridine in the TPEA group increases the Zn^{2+} coordination ability of PNT (Scheme 2).

The selectivity of the fluorescent response of PND and PNT to zinc ions was examined. Competition experiments were conducted to further check the Zn^{2+} selectivity of PND and PNT in the presence of other metal ions, which demonstrates that PND shows a higher selectivity to Zn^{2+} than that of PNT (Figure 6 and Figure S7 in the Supporting Information). As shown in Figure 6, the emission profile of Zn^{2+}–PND complex is unperturbed in the presence of 10 equivalents of Na^+, K^+, Mg^{2+}, and Ca^{2+}, which are physiologically important and abundant cations existing in living cells. More importantly, most heavy and transition-metal ions (HTM ions), including Co^{2+}, Ni^{2+}, Ag^+, Hg^{2+}, Pb^{2+}, and Mn^{2+}, also have a very negligible effect. Only Cu^{2+} and Fe^{2+} quench fluorescence to some extent, which was often met in other metal-ion sensors,[21,22] and Cu^{2+} could be suppressed by the addition of acetylacetone (see Figure S8 in the Supporting Information). Since there are rare examples of PET-based fluorescent sensors that can discriminate Zn^{2+} from Cd^{2+} owing to their closely related properties,[23,24] we are pleased to find that PND exhibits a much higher fluorescence enhancement to Zn^{2+}, which suggests that PND is a Zn^{2+}-selective fluorescence probe that is less affected by Cd^{2+}. PND shows high selectivity toward Zn^{2+} over other competing metal ions in aqueous solution. Unexpectedly, al-

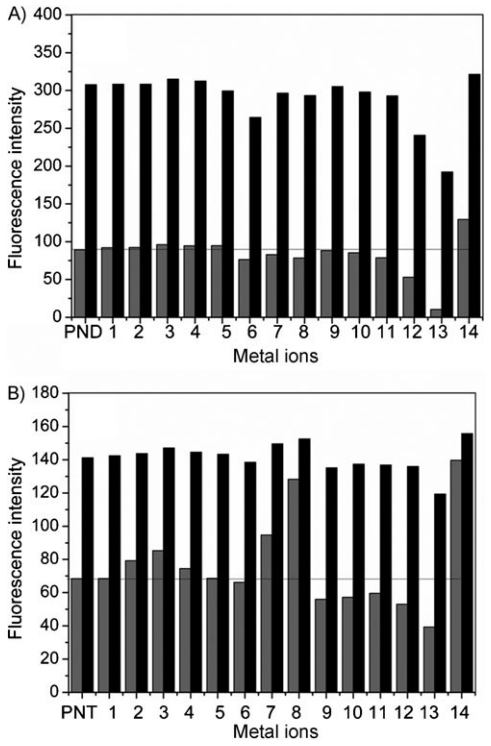

Figure 6. The relative fluorescence intensity at pH 7.00 (10 mM MOPS) of various metal ions: A) PND (λ_{em} = 650 nm, 30 μM). B) PNT (λ_{em} = 630 nm, 30 μM). Light gray bars represent the addition of the analytes: 1) Na^+ (300 μM), 2) K^+ (300 μM), 3) Mg^{2+} (300 μM), 4) Ca^{2+} (300 μM), 5) Cr^{2+} (30 μM), 6) Mn^{2+} (30 μM), 7) Co^{2+} (30 μM), 8) Ni^{2+} (30 μM), 9) Ag^+ (30 μM), 10) Pb^{2+} (30 μM), 11) Hg^{2+} (30 μM), 12) Fe^{2+} (30 μM), 13) Cu^{2+} (30 μM), and 14) Cd^{2+} (30 μM). Black bars represent the subsequent addition of Zn^{2+} (30 μM) to the solution.

though the additional pyridine promotes the stability of Zn^{2+}–PNT complexes, PNT showed less selectivity with less fluorescent enhancement with respect to PND (see Figure S7B in the Supporting Information), and was interfered with by the presence of Co^{2+}, Ni^{2+}, and Cd^{2+}, but with less fluorescent quenching by Fe^{2+} or Cu^{2+} (Figure 6B). As mentioned above, the different selectivity toward the same metal ion (Zn^{2+}) might be also caused by the different binding mode with other HTM ions.

Finally, we apply the NIR sensor of PND to KB cells (human nasopharyngeal epidermal carcinoma cell) for examining whether it could work in living systems with the help of a confocal laser scanning microscopy. Bright-field measurements confirmed that the cells after treatment with Zn^{2+} and PND were viable throughout the imaging experiments (Figure 7A and D). Under selective excitation of PND, staining KB cells with a 20 μM solution of PND for 30 min at 37 °C led to very weak intracellular fluorescence (Figure 7B). After the cells were supplemented with $ZnCl_2$ (20 μM) in the growth medium for 30 min at 37 °C and then loaded with PND under the same conditions, a significant increase in the fluorescence from the intracellular area was observed (Figure 7E). As depicted in Figure 7C and F, the overlay of fluorescence and bright-field images reveals that

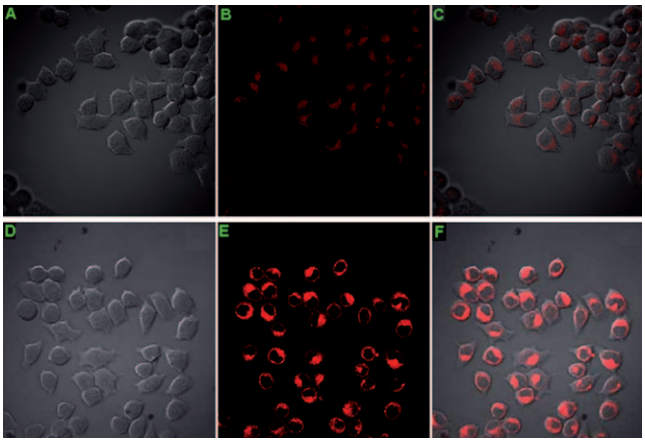

Figure 7. Confocal fluorescence images in KB cells: Top, A–C) Cells incubated with PND (20 μM) for 0.5 h. Bottom, D–F) Cells incubated with $ZnCl_2$ (20 μM) for 0.5 h then PND (20 μM) for 0.5 h. Emission was collected at 598–698 nm upon excitation at 543 nm. Bright field (A and D), fluorescence (B and E), and overlap field (C and F).

the fluorescence signals are localized in the perinuclear area of the cytosol, which indicates a subcellular distribution of Zn^{2+} and good cell-membrane permeability of PND. A similar fluorescence image of PNT was shown in Figure S9 (Supporting Information). These cell experiments demonstrated the usefulness of both PND and PNT for the imaging of Zn^{2+} in living cells.

Conclusion

We have designed and synthesized PND and PNT, two novel and highly sensitive fluorescent probes for Zn^{2+} by using core-substituted naphthalenediimide fluorophore as an NIR fluorophore, and DPEA or TPEA derivatives as Zn^{2+} binding moieties. Interestingly, in the target sensors of PND and PNT, two ionophores exhibit completely different ligand effects on photoinduced electron-transfer (PET) and intramolecular charge transfer (ICT) channels due to the different coordination behavior between DPEA and TPEA. The fluorescence enhancement of PND during the titration with Zn^{2+} is dominated with a typical PET characteristic. In contrast, the N^1 atom for PNT can participate in the coordination of Zn^{2+} ion, diminishing the electron delocalization of the NDI moiety and resulting in the ICT disturbance. For PNT, the distinct blueshift in both absorbance and fluorescence is suggestive of a combination of PET and ICT processes. PND shows several advantages as a probe for sensing Zn^{2+}, such as the determining wavelength falling in the desired NIR region beneficial to high light penetration depth and weak autofluorescence in biological tissues, a PET-based turn-on fluorescent type to get the maximum signal-to-noise ratio, and discriminating Zn^{2+} from Cd^{2+} and other cations apparently through the difference in fluorescence intensity. PND and PNT are long wavelength, cell-permeable, and can be applied to image Zn^{2+} in living cells and in vivo

potentially and should, therefore, be useful for clarifying the roles of Zn^{2+} in biological processes.

Experimental Section

Materials: 1,4,5,8-Naphthalenetetracarboxylic dianhydride was purchased from Tokyo Chemical Industry Co. All other reagents and solvents were purchased from commercial sources and are of analytical grade. *N*,*N*-Di-(pyridin-2-ylmethyl)ethane-1,2-diamine and *N*,*N*,*N*′-tri(pyridin-2-ylmethyl)ethane-1,2-diamine were prepared by the established literature procedure[7c,8].

Apparatus: ^{1}H and ^{13}C NMR in $CDCl_3$ or [D$_6$]DMSO were recorded on a Bruker Avance-400 spectrometer with tetramethylsilane (TMS) as the internal standard. Data for ^{1}H NMR spectra are reported as follows: chemical shift (ppm) and multiplicity (s = singlet, d = doublet, t = triplet, q = quartet, m = multiplet). Data for ^{13}C NMR spectra are reported in ppm. HRMS were measured on a Waters LCT Premier XE spectrometer. UV/Vis spectra were obtained by using a Varian Cary 500 spectrophotometer (1 cm quartz cell) at 25 °C. Fluorescent spectra were recorded on a Varian Cary Eclipse fluorescence spectrophotometer (1 cm quartz cell) at 25 °C. The slit width was 5 nm for both excitation and emission. TLC analyses were performed on silica-gel plates and flash chromatography was conducted by using silica-gel column packages purchased from Qingdao Haiyang Chemical Co. (China). The preparation of 2,6-dibromonaphthalene-1,4,5,8-tetracarboxylic dianhydride (**1**) was conducted according to literature methods.[15]

***N*,*N*′-Di-*n*-butyl-2,6-dibromonaphthalene-1,4,5,8-tetracarboxylic acid bisimide (2)**: The mixture of compound **1** (2.13 g, 5 mmol), *n*-butylamine (1.6 g, 21 mmol), and acetic acid (150 mL) was refluxed for 5 h. After having been cooled to room temperature, the precipitate was filtered and washed with water (300 mL) to give **2** as an orange crystal (3.1 g, 58% yield). ^{1}H NMR (400 MHz, $CDCl_3$, TMS): δ = 9.01 (s, 2H; naphthalene-H), 4.22 (t, J = 8.0 Hz, 4H; $-NCH_2-$), 1.71–1.79 (m, 4H; NCH_2CH_2-), 1.44–1.53 (m, 4H; $-CH_2CH_3$), 1.01 ppm (t, J = 7.2 Hz, 6H; $-CH_2CH_3$); MS (EI$^+$): m/z (%): 538.1 (43), 536.1 (100) $[M]^+$, 534.1 (47).

***N*,*N*′-Di-*n*-butyl-2-(*N*-{2-[bis(pyridin-2-ylmethyl)amino]ethyl})-6-bromonaphthalene-1,4,5,8-tetracarboxylic acid bisimide (3a, BND)**: Compound **2** (108 mg, 0.2 mmol) was added to a solution of *N*,*N*-di(2-pyridylmethyl)ethylenediamine[8] (400 mg, 1.2 mmol) in dry NMP (10 mL), and the mixture was stirred at 60 °C for 70 h. After having been evaporated in vacuo, the residue was dissolved in an aqueous solution of 0.1 M HCl (50 mL) and extracted with dichloromethane (3 × 40 mL). The combined organic layer was washed with saturated brine, dried over anhydrous $MgSO_4$, filtered, and rotary evaporated. The crude product was purified by silica-gel chromatography by using methanol/dichloromethane 1:150 as the elute to afford a dark-red solid (73 mg, 52% yield). R_f = 0.3 (methanol/dichloromethane 1:16); ^{1}H NMR (400 MHz, $CDCl_3$, TMS): δ = 10.31 (s, 1H; −NH), 8.54 (s, 1H; naphthalene-H), 8.44 (d, J = 4.4 Hz, 2H; pyridyl-H), 8.24 (s, 1H; naphthalene-H), 7.72 (d, J = 8.0 Hz, 2H; pyridyl-H), 7.56 (t, J = 8.0 Hz, 2H; pyridyl-H), 7.12 (t, J = 4.4 Hz, 2H; pyridyl-H), 4.17 (t, J = 7.2 Hz, 2H; $-NCH_2-$), 4.07 (t, J = 7.2 Hz, 2H; $-NCH_2-$), 3.89 (s, 4H; CH_2-pyridyl), 3.62 (t, J = 5.6 Hz, 2H; $NHCH_2CH_2-$), 2.97 (t, J = 5.6 Hz, 2H; $NHCH_2CH_2-$), 1.67–1.74 (m, 2H; NCH_2CH_2-), 1.58–1.66 (m, 2H; NCH_2CH_2-), 1.42–1.48 (q, J = 5.6 Hz, 2H; $-CH_2CH_3$), 1.33–1.39 (q, J = 5.6 Hz, 2H; $-CH_2CH_3$), 0.95–0.99 (t, J = 5.6 Hz, 3H; $-CH_2CH_3$), 0.91–0.94 ppm (t, J = 5.6 Hz, 3H; $-CH_2CH_3$); ^{13}C NMR (100 MHz, $CDCl_3$): δ = 13.83, 13.98, 20.33, 20.52, 30.15, 30.24, 40.14, 40.63, 40.67, 52.38, 60.31, 101.02, 119.37, 120.04, 122.23, 123.46, 123.54, 124.41, 126.13, 127.79, 129.43, 131.25, 138.56, 148.97, 151.96, 158.77, 162.88, 163.09, 163.38, 165.88 ppm.

***N*,*N*′-Di-*n*-butyl-2-(*N*-{2-[bis(pyridin-2-ylmethyl)amino]ethyl})-6-(*N*-piperidinyl)naphthalene-1,4,5,8-tetracarboxylic acid bisimide (PND)**: Compound **3** (70 mg, 0.1 mmol), piperidine (170 mg, 2.0 mmol), and TEA (200 μL) was dissolved in a solution of dry NMP (5 mL), and the resulting mixture was stirred at 50 °C for 24 h under an argon atmosphere. After having been evaporated in vacuo, the residue was dissolved in an aqueous solution of 0.1 M HCl (50 mL) and extracted with dichloromethane (3 × 40 mL). The combined organic layer was washed with saturated brine, dried over anhydrous $MgSO_4$, filtered, and rotary evaporated. The crude product was purified by silica-gel chromatography by using methanol/dichloromethane 1:120 as the elute to afford PND as an indigo blue solid (43 mg, 31% yield). R_f = 0.3 (methanol/dichloromethane 1:15); ^{1}H NMR (400 MHz, $CDCl_3$, TMS): δ = 9.88 (s, 1H; −NH), 8.50 (d, J = 4.4 Hz, 2H; pyridyl-H), 8.43 (s, 1H; naphthalene-H), 8.06 (s, 1H; naphthalene-H), 7.80 (d, J = 7.6 Hz, 2H; pyridyl-H), 7.62 (t, J = 7.6 Hz, 2H; pyridyl-H), 7.12 (t, J = 4.4 Hz, 2H; pyridyl-H), 4.26 (t, J = 7.2 Hz, 2H; $-NCH_2-$), 4.16 (t, J = 7.2 Hz, 2H; $-NCH_2-$), 3.95 (s, 4H; CH_2-pyridyl), 3.66 (t, J = 5.6 Hz, 2H; $NHCH_2CH_2-$), 3.32 (s, 4H; piperidinyl-H), 3.02 (t, J = 5.6 Hz, 2H; $NHCH_2CH_2-$), 1.86 (s, 4H; piperidinyl-H), 1.74–1.80 (m, J = 7.2 Hz, 2H; NCH_2CH_2-), 1.74 (s, 2H; piperidinyl-H), 1.69 (m, J = 7.2 Hz, 2H; NCH_2CH_2-), 1.49–1.55 (q, J = 5.6 Hz, 2H; $-CH_2CH_3$), 1.41–1.46 (q, J = 5.6 Hz, 2H; $-CH_2CH_3$), 1.02–1.06 (t, J = 5.6 Hz, 3H; $-CH_2CH_3$), 0.95–0.99 ppm (t, J = 5.6 Hz, 3H; $-CH_2CH_3$); ^{13}C NMR (100 MHz, $CDCl_3$): δ = 13.86, 13.94, 20.35, 20.48, 24.03, 26.18, 30.26, 30.28, 40.07, 40.52, 40.58, 52.53, 53.81, 60.33, 101.10, 111.15, 118.78, 121.96, 122.11, 123.35, 123.69, 124.20, 125.40, 127.04, 136.49, 148.91, 149.60, 151.71, 158.98, 161.88, 162.93, 163.20, 165.94 ppm; HRMS (TOF-ESI$^+$): m/z: calcd for $C_{41}H_{48}N_7O_4^+$: 702.3768 $[M+H^+]$; found: 702.3773; calcd for $C_{41}H_{47}N_7O_4Na^+$: 724.3587 $[M+Na^+]$; found: 724.3589.

***N*,*N*′-Di-*n*-butyl-2-[*N*,*N*,*N*′-tri(pyridin-2-ylmethyl)amino]ethyl-6-(*N*-piperidinyl)naphthalene-1,4,5,8-tetracarboxylic acid bisimide (PNT)**: *N*,*N*,*N*′-Tri(pyridin-2-ylmethyl)ethane-1,2-diamine[7c] (400 mg, 1.2 mmol) in dry NMP (10 mL) was added to a solution of **2** (108 mg, 0.2 mmol) and the resulting mixture was stirred at 60 °C for 70 h. After having been evaporated in vacuo, the residue was dissolved in an aqueous solution of 0.1 M HCl (50 mL) and was extracted with dichloromethane (3 × 40 mL). The combined organic layer was dried with magnesium sulfate, filtered, and evaporated in vacuo. The crude product was purified by silica-gel chromatography by using methanol/dichloromethane 1:120 as the elute to afford a dark-red solid (60 mg), which was redissolved in a solution of dry NMP (5 mL) and piperidine (170 mg, 2.0 mmol). The resulting mixture was stirred at 50 °C for 24 h under an argon atmosphere, and was then evaporated in vacuo. The residue was dissolved in an aqueous solution of 0.1 M HCl (30 mL) and extracted with dichloromethane (3 × 20 mL). The combined organic layer was dried with magnesium sulfate, filtered, and evaporated in vacuo. The crude product was purified by silica-gel chromatography by using methanol/dichloromethane 1:100 as the elute to afford PNT as an indigo/blue solid (30 mg, 23% yield). R_f = 0.3 (methanol/dichloromethane 1:12); ^{1}H NMR (400 MHz, $CDCl_3$, TMS): δ = 8.46 (d, J = 6.0 Hz, 1H; pyridyl-H), 8.45 (s, 1H; naphthalene-H), 8.39 (s, 1H; naphthalene-H), 8.38 (d, J = 6.0 Hz, 2H; pyridyl-H), 7.54 (t, J = 7.6 Hz, 1H; pyridyl-H), 7.46 (t, J = 7.6 Hz, 2H; pyridyl-H), 7.31 (d, J = 7.6 Hz, 1H; pyridyl-H), 7.23 (d, J = 7.6 Hz, 2H; pyridyl-H), 7.09 (t, J = 6.0 Hz, 1H; pyridyl-H), 7.03 (t, J = 6.0 Hz, 2H; pyridyl-H), 4.64 (s, 2H; CH_2-pyridyl), 4.12–4.18 (m, 4H; $-NCH_2-$), 3.68 (s, 4H; CH_2-pyridyl), 3.59 (t, J = 6.0 Hz, 2H; NCH_2CH_2N-), 3.38 (s, 4H; piperidinyl-H), 2.85 (t, J = 6.0 Hz, 2H; NCH_2CH_2N-), 1.83 (s, 4H; piperidinyl-H), 1.65–1.72 (m, 4H; NCH_2CH_2-), 1.60 (s, 2H; piperidinyl-H), 1.35–1.44 (m, 4H; $-CH_2CH_3$), 0.94–0.99 ppm (m, 6H; $-CH_2CH_3$); ^{13}C NMR (100 MHz, $CDCl_3$): δ = 13.85, 13.87, 20.38, 23.99, 29.67, 30.32, 40.59, 40.67, 51.99, 52.46, 53.66, 58.86, 60.56, 109.19, 110.38, 121.93, 122.26, 122.33, 122.88, 124.04, 124.56, 125.06, 125.13, 125.47, 126.58, 136.30, 136.76, 148.86, 149.35, 151.12, 152.28, 157.61, 159.02, 161.77, 161.93, 163.01, 163.17 ppm; HRMS (TOF-ESI$^+$): m/z: calcd for $C_{47}H_{53}N_8O_4^+$: 793.4190 $[M+H^+]$; found: 793.4201; calcd for $C_{47}H_{52}N_8O_4Na^+$: 815.4009 $[M+Na^+]$; found: 815.4001.

UV/Vis absorption spectrum measurements: The absorption spectra of PND (50 μM) were measured at 25 °C in aqueous solution (acetone/100 mM MOPS buffer 90:10, pH 7.0). Zn^{2+} was added as $Zn(NO_3)_2$ (0, 0.1, 0.2, 0.3, 0.4, 0.5, 0.6, 0.7, 0.8, 0.9, 1.0, 1.1, 1.2, and 2.0 equiv of Zn^{2+} with respect to PND). The absorption spectra of PNT (50 μM) were measured under the same conditions.

Fluorescence spectral measurements: The fluorescence spectra of PND (50 μM) were measured at 25 °C in aqueous solution (acetone/100 mM

MOPS buffer 90:10, pH 7.0) upon excitation at $\lambda = 610$ nm. The amounts of Zn^{2+} added were 0, 0.2, 0.4, 0.6, 0.8, 1.0, 1.2, and 1.4 equiv. The fluorescence spectra of PNT (50 μM) were also measured in MOPS buffer at 25 °C upon excitation at the isosbesitic wavelength of $\lambda = 566$ nm.

Quantum yield measurements: The quantum yields of fluorescence were determined by comparison of the integrated area of the corrected emission spectrum with a reference of *N*,*N*′-di(2,6-dibutyl)-1,6,7,12-tetrakis(4-*tert*-butylphenoxy)-3,4:9,10-perylenetetracarboxylic diimide ($\Phi = 0.66$, in CH_2Cl_2).[17] For the metal-free study, 5 mL of 5 μM PND or PNT in aqueous solution (acetone/100 mM MOPS buffer 90:10, pH 7.0) was prepared. For the metal-bound studies, $Zn(NO_3)_2$ (15 μL, 5 mM) was added to PND/PNT (5 mL, 5 μM) in aqueous solution (acetone/100 mM MOPS buffer 90:10, pH 7.0). The reference concentration was adjusted to match the absorbance of a test sample at excitation wavelength. Emission for PND was integrated from 615 to 800 nm with excitation at 610 nm, and PNT was integrated from 576 to 800 nm with excitation at 566 nm. The quantum yields were calculated with the reported expression.[20]

Effect of pH on the fluorescence intensity: The following buffers were used: $ClCH_2COOH/ClCH_2COONa$ buffer (100 mM, pH 3.0 and 3.6), AcOH/AcONa buffer (100 mM, pH 4.2, 4.8, and 5.4), MES buffer (100 mM, pH 5.7, 6.1, and 6.5), MOPS buffer (100 mM, pH 7.0, 7.4, and 8.0), and CHES buffer (100 mM, pH 8.5 and 9.0). The fluorescence intensity ($\lambda_{ex} = 610$, 650 nm) of PND (50 μM) and ($\lambda_{ex} = 566$, 635 nm) PNT were plotted, respectively.[25]

Metal-ion selectivity measurements: The fluorescence selectivity of PND or PNT to various metals was measured in aqueous solution (acetone/100 mM MOPS buffer 90:10, pH 7.0) at 25 °C ($\lambda_{ex} = 610$, 650 nm). Heavy metal ions (30 μM) were added as $AgNO_3$, $Cd(NO_3)_2$, $Hg(NO_3)_2$, $Pb(NO_3)_2$, $MnSO_4$, $FeSO_4$, $NiSO_4$, and $CuSO_4$. Other cations were added as $Zn(NO_3)_2$ (30 μM), $NaNO_3$ (300 μM), KNO_3 (300 μM), $CaCl_2$ (300 μM), and $MgSO_4$ (300 μM).

Cell culture: A human nasopharyngeal epidermal carcinoma cell line (KB cell) was provided by the Institute of Biochemistry and Cell Biology, SIBS, CAS (China). Cells were grown at 37 °C and with 5% CO_2 in Roswell Park Memorial Institute medium (RPMI) 1640 supplemented with 10% fetal bovine serum (FBS). Cells (5×10^8 L^{-1}) were plated on 14 mm glass coverslips under 100% humidity and allowed to adhere for 24 h. The cells were washed three times with PBS buffer, and the medium was replaced with PBS buffer before imaging.

Microscopy and imaging methods: Confocal luminescence imaging: Confocal luminescence imaging of cells was performed with a modified Olympus FV1000 laser-scanning microscope. A 60× oil-immersion objective lens was used. Excitation was carried out with an Ar laser at $\lambda =$ 543 nm, and emissions were collected in the range $\lambda = 598$–698 nm, including the maximum excitation wavelength of PND (650 nm) and PNT (634 nm). KB cells were incubated with a PBS solution of $ZnCl_2$ (20 μM) for 0.5 h, then the cells were incubated with a PBS solution (note: ca. 1% acetonitrile was added for solubility reasons) of PND or PNT (20 μM) for dye loading for 0.5 h at 37 °C. The stained cells were washed three times with PBS buffer, and the medium was replaced with PBS buffer before imaging. Then the treated cells were imaged by fluorescence microscopy.

Computational details (LANL2DZ-optimized geometries of PND–Zn^{2+} and PNT–Zn^{2+}): The DFT calculations were carried out by using a Gaussian 03 software package.[26] The ground-state geometries of PND–Zn^{2+} and PNT–Zn^{2+} were optimized at the DFT level with the B3LYP hybrid functional in combination with the LANL2DZ basis set for the Zn atom and the D95V basis set for C, H, O, and N atoms.

Acknowledgements

This work was financially supported by the NSFC/China, National Basic Research 973 Project (2006CB806200), Project for New Century Excellent Talents in University (NCET-06-0418), Shanghai Shuguang Project (07SG34), Specialized Research Fund for the Doctoral Program of Higher Education (SRFDP 200802510011), and the State Key Laboratory of Precision Spectroscopy (ECNU).

[1] a) J. M. Berg, Y. G. Shi, *Science* **1996**, *271*, 1081–1085; b) J. J. R. Frausto da Silva, R. J. P. Williams in *The Biological Chemistry of the Elements*, Oxford University Press, New York, **2001**, pp. 315–335; c) M. Dhanasekaran, S. Negi, Y. Sugiura, *Acc. Chem. Res.* **2006**, *39*, 45–52; d) S. F. Sousa, P. A. Fernandes, M. J. Ramos, *J. Am. Chem. Soc.* **2007**, *129*, 1378–1385; e) D. D. Mott, M. Benveniste, R. J. Dingledine, *J. Neurosci.* **2008**, *28*, 1659–1671.

[2] a) A. I. Bush, *Trends Neurosci.* **2003**, *26*, 207–214; b) D. Noy, I. Solomonov, O. Sinkevich, T. Arad, K. Kjaer, I. Sagi, *J. Am. Chem. Soc.* **2008**, *130*, 1376–1383.

[3] For recent examples of fluorescent probes for the zinc ion: a) M. S. Park, K. M. K. Swamy, Y. J. Lee, H. N. Lee, Y. J. Jang, Y. H. Moon, J. Yoon, *Tetrahedron Lett.* **2006**, *47*, 8129–8132; b) A. Ojida, Y. Mito-Oka, M. Inoue, I. Hamachi, *J. Am. Chem. Soc.* **2002**, *124*, 6256–6258; c) M. Taki, J. L. Wolford, T. V. O'Halloran, *J. Am. Chem. Soc.* **2004**, *126*, 712–713; d) A. Harriman, L. J. Mallon, B. Stewart, G. Ulrich, R. Ziessel, *Eur. J. Org. Chem.* **2007**, 3191–3198; e) K. Komatsu, Y. Urano, H. Kojima, T. Nagano, *J. Am. Chem. Soc.* **2007**, *129*, 13447–13454; f) P. Jiang, L. Chen, J. Lin, Q. Liu, J. Ding, X. Gao, Z. Guo, *Chem. Commun.* **2002**, 1424–1425; g) B. A. Wong, S. Friedle, S. J. Lippard, *Inorg. Chem.* **2009**, *48*, 7009–7011; h) Z. Xu, X. Qian, J. Cui, R. Zhang, *Tetrahedron* **2006**, *62*, 10117–10122; i) F. Qian, C. Zhang, Y. Zhang, W. He, X. Gao, P. Hu, Z. Guo, *J. Am. Chem. Soc.* **2009**, *131*, 1460–1468; j) Y. Liu, N. Zhang, Y. Chen, L. H. Wang, *Org. Lett.* **2007**, *9*, 315–318; k) P. Carol, S. Sreejith, A. Ajayaghosh, *Chem. Asian J.* **2007**, *2*, 338–348; l) K. K. Upadhyay, A. Kumar, J. Zhao, R. K. Mishra, *Talanta* **2010**, *81*, 714–721.

[4] E. M. Nolan, S. J. Lippard, *Acc. Chem. Res.* **2009**, *42*, 193–203.

[5] a) K. Kiyose, H. Kojima, Y. Urano, T. Nagano, *J. Am. Chem. Soc.* **2006**, *128*, 6548–6549; b) B. Tang, H. Huang, K. Xu, L. Tong, G. Yang, X. Liu, L. An, *Chem. Commun.* **2006**, 3609–3611; c) C.-H. Hung, G.-F. Chang, A. Kumar, G.-F. Lin, L.-Y. Luo, W.-M. Ching, E. W.-G. Diau, *Chem. Commun.* **2008**, 978–980; d) S. Atilgan, T. Ozdemir, E. U. Akkaya, *Org. Lett.* **2008**, *10*, 4065–4067.

[6] J. Fan, X. Peng, Y. Wu, E. Lu, H. Zhang, *J. Lumin.* **2005**, *114*, 125–130.

[7] a) E. Kawabata, K. Kikuchi, Y. Urano, H. Kojima, A. Odani, T. Nagano, *J. Am. Chem. Soc.* **2005**, *127*, 818–819; b) O. Horner, J. J. Girerd, C. Philouze, L. Tchertanov, *Inorg. Chim. Acta* **1999**, *290*, 139–144; c) C. Hureau, S. Groni, R. Guillot, G. Blondin, C. Duboc, E. Anxolabéhère-Mallart, *Inorg. Chem.* **2008**, *47*, 9238–9247; d) Z. Xu, G.-H. Kim, S. Han, M. Jou, C. Lee, I. Shin, J. Yoon, *Tetrahedron* **2009**, *65*, 2307–2312.

[8] a) W. Jiang, Q. Fu, H. Fan, W. Wang, *Chem. Commun.* **2008**, 259–261; b) A. P. de Silva, H. Q. N. Gunaratne and C. P. McCoy, *Chem. Commun.* **1996**, 2399; c) S. A. de Silva, A. Zavaleta, D. E. Baron, O. Allam, E. V.Isidor; N. Kashimura; J. M. Percarpio, *Tetrahedron Lett.* **1997**, *38*, 2237–2240.

[9] a) K. Hanaoka, Y. Muramatsu, Y. Urano, T. Terai, T. Nagano, *Chem. Eur. J.* **2009**, *15*, 568–572; b) V. Amendola, M. Boiocchi, V. Brega, L. Fabbrizzi, L. Mosca, *Inorg. Chem.* **2010**, *49*, 997–1007; c) M. Boiocchi, L. Fabbrizzi, M. Garolfi, M. Licchelli, L. Mosca, C. Zanini, *Chem. Eur. J.* **2009**, *15*, 11288–11297.

[10] a) N. Ashkenasy, W. S. Horne, M. R. Ghadiri, *Small* **2006**, *2*, 99–102; b) G. D. Pantoş, P. Pengo, J. K. M. Sanders, *Angew. Chem.* **2007**, *119*, 198–201; *Angew. Chem. Int. Ed.* **2007**, *46*, 194–197; c) A. L. Sisson, N. Sakai, N. Banerji, A. Fürstenberg, E. Vauthey, S. Matile, *Angew. Chem.* **2008**, *120*, 3787–3789; *Angew. Chem. Int. Ed.* **2008**, *47*, 3727–3729; d) N. Sakai, R. K. Kishore, S. Matile, *Org. Biomol. Chem.* **2008**, *6*, 3970–3976; e) R. Bhosale, A. P. Velasco, V. Ravikumar, R. K. Kishore, O. Kel, A. G. Casado, P. Jonkheijm, J. Huskens, P. Maroni, M. Borkovec, T. Sawada, E. Vauthey, N. Sakai, S. Matile, *Angew. Chem.* **2009**, *121*, 6583–6586; *Angew. Chem. Int. Ed.* **2009**, *48*, 6461–6464; f) N. Kimizuka, T. Kawasaki, K. Hirata, T. Kunitake, *J. Am. Chem. Soc.* **1995**, *117*, 6360–6361.

[11] a) F. Würthner, *Angew. Chem.* **2001**, *113*, 1069–1071; *Angew. Chem. Int. Ed.* **2001**, *40*, 1037–1039; b) T. B. Singh, S. Erten, S. Gunes, C. Zafer, G. Turkmen, B. Kuban, Y. Teoman, N. S. Sariciftci, S. Icli, *Org. Electron.* **2006**, *7*, 480–489; c) K. Hizu, T. Sekitani, T. Someya, J. Otsuki, *Appl. Phys. Lett.* **2007**, *90*, 093504.

[12] a) R. F. Kelley, M. J. Tauber, M. R. Wasielewski, *J. Am. Chem. Soc.* **2006**, *128*, 4779–4791; b) M. R. Wasielewski, *J. Org. Chem.* **2006**, *71*, 5051–5066; c) L. Flamigni, E. Baranoff, J. P. Collin, J. P. Sauvage, *Chem. Eur. J.* **2006**, *12*, 6592–6606; d) B. C. Thompson, J. M. J. Fréchet, *Angew. Chem.* **2008**, *120*, 62–82; *Angew. Chem. Int. Ed.* **2008**, *47*, 58–77.

[13] a) M. Licchelli, A. O. Biroli, A. Poggi, *Org. Lett.* **2006**, *8*, 915–918; b) H. N. Lee, Z. Xu, S. K. Kim, K. M. K. Swamy, Y. Kim, S.-J. Kim, J. Yoon, *J. Am. Chem. Soc.* **2007**, *129*, 3828–3829.

[14] a) S. Chopin, F. Chaignon, E. Blart, F. Odobel, *J. Mater. Chem.* **2007**, *17*, 4139–4146; b) F. Würthner, S. Ahmed, C. Thalacker, T. Debaerdemaeker, *Chem. Eur. J.* **2002**, *8*, 4742–4750; c) R. S. K. Kishore, O. Kel, N. Banerji, D. Emery, G. Bollot, J. Mareda, A. G. Casado, P. Jonkheijm, J. Huskens, P. Maroni, M. Borkovec, E. Vauthey, N. Sakai, S. Matile, *J. Am. Chem. Soc.* **2009**, *131*, 11106–11116.

[15] F. Chaignon, M. Falkenstrom, S. Karlsson, E. Blart, F. Odobel, L. Hammarstrom, *Chem. Commun.* **2007**, 64–66.

[16] S. V. Bhosale, C. H. Jani, S. J. Langford, *Chem. Soc. Rev.* **2008**, *37*, 331–342.

[17] J. H. Hurenkamp, W. R. Browne, R. Augulis, A. Pugzlys, P. H. M. van Loosdrecht, J. H. van Esch, B. L. Feringa, *Org. Biomol. Chem.* **2007**, *5*, 3354–3362.

[18] H. He, M. A. Mortellaro, M. J. Leiner, S. T. Young, R. J. Fraatz, G. Anderegg, *Anal. Chem.* **2003**, *75*, 549–555.

[19] E. Ballesteros, D. Moreno, T. Gomez, T. Rodriguez, J. Rojo, M. Garcia-Valverde, T. Torroba, *Org. Lett.* **2009**, *11*, 1269–1272.

[20] Z. Xu, K. Baek, H. Kim, J. Cui, X. Qian, D. Spring, I. Shin, J. Yoon, *J. Am. Chem. Soc.* **2010**, *132*, 601–610.

[21] X. J. Peng, J. J. Du, J. L. Fan, J. Y. Wang, Y. K. Wu, J. Z. Zhao, S. G. Sun, T. Xu, *J. Am. Chem. Soc.* **2007**, *129*, 1500–1501.

[22] H. Wang, Q. Gan, X. Wang, L. Xue, S. Liu, H. Jiang, *Org. Lett.* **2007**, *9*, 4995–4998.

[23] J. N. Ngwendson, A. Banerjee, *Tetrahedron Lett.* **2008**, *49*, 7316–7319.

[24] T. Cheng, Y. Xu, S. Zhang, W. Zhu, X. Qian, L. Duan, *J. Am. Chem. Soc.* **2008**, *130*, 16160–16161.

[25] T. Hirano, K. Kikuchi, Y. Urano, T. Higuchi, T. Nagano, *J. Am. Chem. Soc.* **2000**, *122*, 12399–12400.

[26] Gaussian 03, Revision C.02, M. J. Frisch, G. W. Trucks, H. B. Schlegel, G. E. Scuseria, M. A. Robb, J. R. Cheeseman, J. A. Montgomery, Jr., T. Vreven, K. N. Kudin, J. C. Burant, J. M. Millam, S. S. Iyengar, J. Tomasi, V. Barone, B. Mennucci, M. Cossi, G. Scalmani, N. Rega, G. A. Petersson, H. Nakatsuji, M. Hada, M. Ehara, K. Toyota, R. Fukuda, J. Hasegawa, M. Ishida, T. Nakajima, Y. Honda, O. Kitao, H. Nakai, M. Klene, X. Li, J. E. Knox, H. P. Hratchian, J. B. Cross, V. Bakken, C. Adamo, J. Jaramillo, R. Gomperts, R. E. Stratmann, O. Yazyev, A. J. Austin, R. Cammi, C. Pomelli, J. W. Ochterski, P. Y. Ayala, K. Morokuma, G. A. Voth, P. Salvador, J. J. Dannenberg, V. G. Zakrzewski, S. Dapprich, A. D. Daniels, M. C. Strain, O. Farkas, D. K. Malick, A. D. Rabuck, K. Raghavachari, J. B. Foresman, J. V. Ortiz, Q. Cui, A. G. Baboul, S. Clifford, J. Cioslowski, B. B. Stefanov, G. Liu, A. Liashenko, P. Piskorz, I. Komaromi, R. L. Martin, D. J. Fox, T. Keith, M. A. Al-Laham, C. Y. Peng, A. Nanayakkara, M. Challacombe, P. M. W. Gill, B. Johnson, W. Chen, M. W. Wong, C. Gonzalez, J. A. Pople, Gaussian, Inc., Wallingford, CT, **2004**.

Received: February 22, 2010
Published online: June 11, 2010

